International Journal of Fracture **48**: 23–40, 1991.
© 1991 *Kluwer Academic Publishers. Printed in the Netherlands.*

Temperature rise in a viscoplastic material during dynamic crack growth

R. KRISHNA KUMAR[1], R. NARASIMHAN[2] and O. PRABHAKAR[1]
[1] *Departments of Mechanical Engineering and Metallurgical Engineering, IIT, Madras 600036, India;*
[2] *Department of Mechanical Engineering, IIT, Bombay 400076, India*

Received 15 February 1989; accepted in revised form 2 January 1990

Abstract. Dynamic steady-state crack growth has been analyzed under mode I plane stress, small-scale yielding conditions using a finite element procedure. A Perzyna type viscoplastic constitutive equation has been employed in this analysis. The viscoplastic work rate is converted into heat input and the temperature distribution is determined by solving the governing conduction/convection equation also by a finite element method. The *Stream-line Upwinding Petrov-Galerkin* formulation has been employed for this purpose because of the high Péclet number that results in such a type of analysis. The effect of strain rate sensitivity and crack speed on the temperature distribution near the crack tip is examined.

1. Introduction

Temperature rise during dynamic crack growth in ductile materials occurs because the plastic work is converted into heat. It is important to investigate this temperature rise because it may affect the material behaviour. Also, it may have a significant influence on the fracture toughness values. Some early experiments by Krafft and Irwin [1] and Eftis and Krafft [2] on fracture toughness display the influence of temperature. Krafft and Irwin [1] found that the fracture toughness of a 6A1-4V titanium alloy increased steadily with loading rate, when tests were conducted at room temperature. However, a minimum in fracture toughness occurred when the test was conducted at a temperature higher than the room temperature. Eftis and Krafft [2] observed (by using a combined rate scale) that a minimum in fracture toughness for mild steel is reached for a crack velocity that is only a small fraction of the elastic wave speed. As pointed out by Rice and Levy [3], it is difficult to believe that this could be caused by inertia alone.

Recognizing the above factors, Rice and Levy [3] calculated the temperature rise in mode I crack growth using the Dugdale model. It was found that the Dugdale model predicts very high temperatures because of a large concentration of plastic straining directly ahead of the crack tip. Weichert and Schonert [4, 5] determined the temperature distribution for a steady-state crack growth condition by treating the crack tip as a moving heat source. They considered both a circular as well as a rectangular heat source and found the temperature rise to be of the order of 1000°C for brittle materials. Kuang and Atluri [6] used a finite element procedure with a moving mesh to predict the temperature rise. They assumed the heat source to be either uniform or to have a $1/r$ singularity. Also, they considered the total strength of the heat source to be a constant. Within the above framework, they allowed the crack to grow at different velocities and computed the temperature rise, which was found to be of the order of 1000°C.

Douglas and Mair [7] used the asymptotic fields for mode III dynamic crack propagation and estimated the temperature rise near the crack tip. The constitutive equation was assumed to be elastic-perfectly plastic. They concluded that the relative temperature rise decreases with increasing crack velocity. Malali [8] conducted a finite element analysis to calculate the stress and strain fields near the crack tip during dynamic crack propagation under mode III small-scale yielding conditions in an elastic-perfectly plastic material. The temperature rise was then computed using the integral based on superposition of heat sources given by Carslaw and Jaeger [9] which was also employed by Rice and Levy [3].

Experimental measurement of the temperature rise at the vicinity of a rapidly propagating crack tip is extremely difficult. This is because a material point attains the maximum temperature in a few micro-seconds. Also, the temperature rise during crack growth is confined to a very small region near the crack tip. Fuller, Fox and Field [10] measured temperatures in PMMA material using thermocouples and a temperature sensitive liquid crystal film as well as by an infrared detector. They found that the temperature rise is almost a constant for a range of velocities varying from 200–650 ms^{-1} and is approximately 500°C. Weichert and Schonert [5] measured the temperature rise in glass and quartz using a very sensitive radiation thermometer. In a very recent study, Zehnder and Rosakis [11] have employed high speed, high resolution, non-contact infrared sensors to detect the temperature rise during rapid crack growth in a 4340 carbon steel. In their initial experiments, they measured a temperature rise of about 450°C close to the crack tip. A number of attempts have also been made to estimate the temperature increase under fatigue loading conditions [12, 13].

Theoretical and numerical studies of the mechanics problem of dynamic crack propagation have been performed by a number of researchers [14–19]. Freund and Douglas [14] examined the asymptotic fields for anti-plane shear crack growth in a rate independent elastic-plastic material under steady-state conditions. They also showed that the dynamic fracture toughness is a strong function of the velocity of crack growth. A similar analysis for mode I plane strain was undertaken by Lam and Freund [15]. Asymptotic crack tip fields were studied theoretically by Slepyan [16], Achenbach and Dunayevsky [17], Gao and Nemat-Nasser [18] and Guo et al. [19].

The effect of material rate sensitivity in dynamic fracture has been well recognized [20–24]. Lo [20] obtained the asymptotic stress and strain variations for a rate sensitive plastic material during dynamic crack growth under both anti-plane shear and plane strain conditions. Freund and Hutchinson [21] and Freund et al. [22] have used a high strain rate constitutive equation to study steady-state dynamic crack growth under mode I plane strain. They employed an approximate analytical technique in the earlier work [21] and subsequently validated the results by a finite element analysis [22]. Brickstad [23] used a Perzyna type [25] viscoplastic constitutive equation to analyze transient crack growth experiments in a cold rolled steel. Freund and Douglas [24] have examined the effect of rate sensitivity on the relationship between dynamic fracture toughness and crack velocity under mode III using a finite element analysis.

From the above review, it may be observed that very little research work has been devoted to studying the effect of strain rate sensitivity on the temperature rise near the crack tip during rapid crack propagation. Rice and Levy [3] have underscored the importance of taking into account the increase in flow stress with strain rate (since the strain rates

experienced by material points close to the growing crack tip are large) in the temperature rise calculations. As a first step in this direction, Sung and Achenbach [26] have used a plane strain solution to estimate the peak temperature near a dynamically propagating crack tip in a viscoplastic material. Also, the above review indicates that no attempt has thus far been made to determine the temperature rise using a (consistent) finite element analysis to solve both the mechanics and thermal problems.

In this paper, a finite element analysis has been performed to study the stress and strain fields near a steadily propagating crack tip as well as the temperature distribution around the tip. Plane stress, mode I small-scale yielding conditions together with a viscoplastic constitutive equation of the Perzyna type have been assumed in this analysis. The particular material properties that have been used here to report the results correspond to the cold rolled steel employed by Brickstad [23]. Section 2.1 of this paper explains the numerical procedure for solving the mechanics problem and 2.2 the numerical procedure for solving the thermal problem. Results and discussions are given in Section 3.

2. Numerical procedure

2.1. The mechanics problem

In this paper, steady state dynamic crack growth under mode I, plane stress, small-scale yielding conditions has been simulated using the finite element procedure employed by Lam and Freund [15] and Freund and Douglas [14]. A semi-infinite crack is assumed to grow with velocity v in an unbounded body such that the zone of inelastic deformation is contained in a small region near the crack tip and the elastodynamic K-field [27] holds good at points far away from the crack tip. The essential features of this formulation are outlined below. A more detailed description may be found in [14, 15].

The equations of motion with respect to a set of Cartesian coordinates x_1, x_2 centered at the crack tip and translating with it may be written as

$$\frac{\partial \sigma_{\alpha\beta}}{\partial x_\beta} = \rho v^2 \frac{\partial^2 u_\alpha}{\partial x_1^2}, \tag{1}$$

where $\sigma_{\alpha\beta}$ is the stress tensor, u_α is the displacement vector and ρ is the mass density of the material. Standard tensor notation is employed here, with repeated indices implying summation. Further, Greek indices such as α, β, γ etc. have the range 1, 2. The crack has been assumed to grow in the x_1 direction with velocity v and the steady state condition, $\partial(\ )/\partial t = (\dot{\ }) = -v\partial(\ )/\partial x_1$, has been used to arrive at the above equation.

In order to simplify further development, the crack tip coordinates and field quantities are normalized as

$$\left.\begin{aligned} \hat{x}_\alpha &= x_\alpha/(K/\sigma_0)^2 \\ \hat{u}_\alpha &= u_\alpha/(K^2/E\sigma_0) \\ \hat{\varepsilon}_{\alpha\beta} = \varepsilon_{\alpha\beta}/\varepsilon_0 \quad &\text{and} \quad \hat{\sigma}_{\alpha\beta} = \sigma_{\alpha\beta}/\sigma_0 \end{aligned}\right\}. \tag{2}$$

Here, σ_0 is the initial yield stress, $\varepsilon_0 = \sigma_0/E$ is the initial yield strain, E is the Young's modulus and K is the remote dynamic stress intensity factor. Also, $m_s = v/c_s$ will denote a normalized crack speed, where $c_s = (\mu/\rho)^{1/2}$ is the elastic shear wave speed and μ is the shear modulus of the material.

Using the above normalizations, the equilibrium equation (1) may be rewritten as

$$\frac{\partial \hat{\sigma}_{\alpha\beta}}{\partial \hat{x}_\beta} = \frac{1}{2(1+\nu)} m_s^2 \frac{\partial^2 \hat{u}_\alpha}{\partial \hat{x}_1^2}, \tag{3}$$

where ν is the Poisson's ratio. An additive decomposition of the small strain tensor is assumed as

$$\hat{\varepsilon}_{\alpha\beta} = \hat{\varepsilon}^e_{\alpha\beta} + \hat{\varepsilon}^p_{\alpha\beta}, \tag{4}$$

where $\hat{\varepsilon}^e_{\alpha\beta}$ is the normalized elastic strain and $\hat{\varepsilon}^p_{\alpha\beta}$ is the normalized viscoplastic strain. The normalized stresses are related to the normalized elastic strains by

$$\hat{\sigma}_{\alpha\beta} = \hat{C}_{\alpha\beta\gamma\delta}\hat{\varepsilon}^e_{\gamma\delta}, \tag{5}$$

where $\hat{C}_{\alpha\beta\gamma\delta}$ is the elasticity tensor divided by the Young's modulus E.

A virtual work representation of (3) may be written as [15]

$$\int_V \left(\delta\hat{\varepsilon}_{\alpha\beta}\hat{C}_{\alpha\beta\gamma\delta}\hat{\varepsilon}_{\gamma\delta} - \frac{m_s^2}{2(1+\nu)} \frac{\partial(\delta\hat{u}_\alpha)}{\partial \hat{x}_1} \frac{\partial \hat{u}_\alpha}{\partial \hat{x}_1} \right) \mathrm{d}V = \int_V \delta\hat{\varepsilon}_{\alpha\beta}\hat{C}_{\alpha\beta\gamma\delta}\hat{\varepsilon}^p_{\gamma\delta}\, \mathrm{d}V$$

$$+ \int_{S_T} \delta\hat{u}_\alpha \left(\hat{T}_\alpha - \frac{m_s^2}{2(1+\nu)} \frac{\partial \hat{u}_\alpha}{\partial \hat{x}_1} n_1 \right) \mathrm{d}S. \tag{6}$$

Here, $\delta\hat{\varepsilon}_{\alpha\beta}$ is the virtual strain tensor and $\hat{T}_\alpha$ is the normalized traction vector acting on the portion S_T of the boundary (of the domain V) whose outward normal is n_α.

By applying the usual procedure, the finite element equilibrium equations may be obtained from (6) as

$$\mathbf{KU} = \mathbf{F} + \mathbf{R}. \tag{7}$$

The stiffness matrix $\mathbf{K}$ and the force vectors $\mathbf{F}$ and $\mathbf{R}$ in the above equation are defined as follows:

$$\left.\begin{aligned} \mathbf{K} &= \int_V \mathbf{B}^T\hat{\mathbf{C}}\mathbf{B}\, \mathrm{d}V - \frac{m_s^2}{2(1+\nu)} \int_V \frac{\partial \mathbf{N}^T}{\partial \hat{x}_1} \frac{\partial \mathbf{N}}{\partial \hat{x}_1}\, \mathrm{d}V \\ \mathbf{F} &= \int_{S_T} \mathbf{N}^T \left(\hat{\mathbf{T}} - \frac{m_s^2}{2(1+\nu)} \frac{\partial \hat{\mathbf{u}}}{\partial \hat{x}_1} n_1 \right) \mathrm{d}S \\ \mathbf{R} &= \int_V \mathbf{B}^T\hat{\mathbf{C}}\hat{\boldsymbol{\varepsilon}}^p\, \mathrm{d}V \end{aligned}\right\}. \tag{8}$$

In the above equations, **U** is the vector of nodal point displacements, **N** is the shape function matrix and **B** is the strain displacement matrix. In the present study, rectangular four-noded isoparametric elements were employed with bilinear shape functions. No attempt has been made to incorporate the singularity of the strains by using special crack tip elements in order to avoid unnecessary ambiguity in the solution.

The constitutive equation used here is the one suggested by Perzyna [25], which assumes that the viscoplastic strain rate is a function of the *over-stress*. The particular form of this constitutive law that is employed is given by

$$\dot{\varepsilon}_{ij}^{p} = \beta\phi r_{ij} = \dot{\gamma} r_{ij}, \tag{9}$$

where β is a viscosity parameter, ϕ is the over-stress function, $\dot{\gamma}$ is the rate of plastic flow and r_{ij} is the flow direction. The over-stress function ϕ and the flow vector r_{ij} are chosen as

$$\left.\begin{aligned} \phi &= \left(\frac{\bar{\sigma} - \sigma_0}{\sigma_0}\right)^n \\ r_{ij} &= \frac{3s_{ij}}{2\bar{\sigma}} \end{aligned}\right\}. \tag{10}$$

In the above equation, s_{ij} is the deviatoric stress tensor, $\bar{\sigma} = \sqrt{3J_2}$ is the Mises equivalent stress and n is the rate exponent. Here, J_2 represents the second invariant of deviatoric stress tensor. Equation (9) can be expressed using the normalization (2) as

$$\frac{\partial \hat{\varepsilon}_{ij}^{p}}{\partial \hat{x}_1} = -\beta^* \phi r_{ij} = \frac{\partial \hat{\gamma}}{\partial \hat{x}_1} r_{ij}, \tag{11}$$

where $\beta^* = (EK^2\beta/\sigma_0^3 v)$. In this small-scale yielding formulation, the normalized parameter β^* characterizes the degree of rate sensitivity. For fixed crack speed v, a small value of β^* implies that either β is small or K (i.e., the plastic zone size) is small. Hence, at a certain $(\hat{x}_1, \hat{x}_2)$, rate effects are expected to be stronger for smaller β^*.

The important difference in the numerical formulation for rate independent and rate dependent materials is the stress update algorithm. The stress update procedure used here is the rate tangent modulus method due to Pierce, Shih and Needleman [28]. Their algorithm was developed to integrate forward in time rate equations of the form (9), to obtain the total viscoplastic strains and stresses. However, in the present formulation, the total viscoplastic strain at a certain point $(\hat{x}_1, \hat{x}_2)$ is obtained by integrating equation (11) from the elastic-plastic boundary, in the negative $\hat{x}_1$ direction, along a line holding $\hat{x}_2$ constant. The initial state of the material outside the elastic-plastic boundary is made use of in completing the above integration. The normalized incremental plastic flow at a certain integration station $\hat{x}_1^{m+1}$ along the *integration path* may be obtained by a Taylor series expansion about the previous point $\hat{x}_1^m$ as [29]

$$\Delta\hat{\gamma} = \left[-\frac{\Delta\hat{x}_1^m \beta^* \phi_m}{(1+\chi)} + \frac{\chi t_m^r \beta^*}{(1+\chi)} \hat{\boldsymbol{\eta}}_m : \hat{\mathbf{C}} : \Delta\hat{\boldsymbol{\varepsilon}}_m\right]. \tag{12}$$

The parameters χ and t_m^r and the vector $\hat{\boldsymbol{\eta}}_m$ which enter the above equation are defined as

$$\chi = -\frac{\theta \Delta \hat{x}_1^m}{t_m^r}; \quad t_m^r = \frac{1}{\beta^*(\hat{\boldsymbol{\eta}}_m : \hat{\mathbf{C}} : \mathbf{r}_m)}; \quad \hat{\boldsymbol{\eta}}_m = \left(\frac{\partial \phi}{\partial \hat{\boldsymbol{\sigma}}}\right)_m. \tag{13}$$

As noted earlier, the vector $\mathbf{r}_m$ represents the flow direction (see (10)). The parameter θ in the above equation is chosen as 0.5 in the present study which corresponds to the trapezoidal rule [28, 29].

A large rectangular domain is modelled with the outer dimensions more than ten times the size of the crack tip plastic zone. Traction and/or displacement boundary conditions based on the elastodynamic K-field [27] are specified along the outer boundary of the domain. It is to be noted that the stiffness matrix in (8) is only a function of the crack speed and the elastic material properties and hence needs to be factorized only once for a given crack speed m_s. On the other hand, the force vector contains the plastic strains as one of its constituents. In order to solve the non-linear equation (7), an iterative procedure has to be employed as indicated by Freund and Douglas [24]. The solution is started from $\beta^* = 0$ (elastic case), and the value of β^* is gradually increased.

2.2. The thermal problem

In order to determine the temperature distribution, the thermal problem is solved in conjunction with the mechanics problem. The work rate is calculated after solving the mechanics problem and is used as heat input in the heat conduction equation. The governing heat conduction equation is given by

$$\frac{k}{\rho c_p} \nabla^2 T + \frac{Q}{\rho c_p} = \frac{\partial T}{\partial t}, \tag{14}$$

where k is the thermal conductivity, c_p is the specific heat, T is the temperature and $Q = \sigma_{ij} \dot{\varepsilon}_{ij}^p$ is the heat input. On making use of the normalizations given in (2), the above equation reduces to

$$D\left(\frac{\partial^2 T}{\partial \hat{x}_1^2} + \frac{\partial^2 T}{\partial \hat{x}_2^2}\right) + H\hat{Q} = -m_s \frac{\partial T}{\partial \hat{x}_1}, \tag{15}$$

where

$$H = \frac{m_s \sigma_0^2}{E \rho c_p}; \quad D = \frac{E \beta k}{(c_s \sigma_0 \beta^* c_p \rho v)},$$

$$\hat{Q} = -\hat{\sigma}_{ij} \frac{\partial \hat{\varepsilon}_{ij}^p}{\partial \hat{x}_1}.$$

In the above equation, $\hat{Q}$ denotes the *normalized heat input* and D is a normalized thermal diffusivity parameter.

Equation (15) is a convection/diffusion equation whose solution characteristics are governed by the Péclet number $m_s h/D$, where h is the finite element mesh size. It should be noted that the Péclet number for the current problem is very high and ranges from 10^3–10^5. It is well known that such large Péclet numbers give rise to oscillations in the solution [30], when the convection/diffusion equation is solved by the conventional Galerkin finite element formulation.

In order to eliminate oscillations, the *Stream-line Upwinding Petrov-Galerkin* method, suggested by Brooks and Hughes [31] has been used to solve the heat transfer equation (15). In this method, the weighting function belongs to a function space which is different from that of the trial function. The weighting function is modified to weight the element upwind of a node more heavily than the downwind element. Also, unlike the conventional Galerkin method, the *Stream-line Upwind Petrov-Galerkin* method requires a discontinuous weighting function of the form [31]

$$\tilde{W} = W + p. \tag{16}$$

Here, W is the regular continuous weighting function and p is the *stream-line* weighting function which is discontinuous at the inter-element boundary and is given in [31].

For the rectangular element that is used, the weighted residual formulation of (15) becomes

$$\int_V W\left(m_s \frac{\partial T}{\partial \hat{x}_1}\right) \mathrm{d}V - \int_V \nabla W : (D\nabla T)\, \mathrm{d}V$$

$$+ \sum_e \int_{V^e} p\left(m_s \frac{\partial T}{\partial \hat{x}_1} + H\hat{Q}\right) \mathrm{d}V^e + \int_V W(H\hat{Q})\, \mathrm{d}V = 0, \tag{17}$$

where the summation in the third term is carried out over all the elements in the mesh. It must be noted that the above formulation affects the weighting function of the convection term but not that of the conduction term. Also, the stiffness matrix which is obtained when the above equation is converted into a finite element formulation is unsymmetric and consists of two terms. The first term is the contribution from thermal conduction and the second one is due to convection. The boundary conditions for the thermal problem were chosen such that the material is at room temperature in the purely elastic region outside the plastic zone and the temperature gradient across the downstream boundary of the mesh far behind the crack tip was assumed to be zero.

In the problem studied, the viscoplastic constitutive properties as determined by Brickstad [23] for a cold rolled steel specimen have been used. These are given below:

$$\beta = 4.1 \times 10^3\ \mathrm{s}^{-1},$$

$$n = 2,$$

$$E = 2.1 \times 10^5\ \mathrm{MPa},$$

$$\sigma_0 = 1485\ \mathrm{MPa},$$

$$\rho = 7800\ \mathrm{kg\,m}^{-3}.$$

The values of k and c_p were chosen as $45\,\mathrm{N\,s^{-1}\,°C^{-1}}$ an $480\,\mathrm{J\,kg^{-1}\,°C^{-1}}$ respectively. The value of the normalized strain rate sensitivity parameter β^* was varied from 5 to 400 for crack speeds m_s of 0.1, 0.3 and 0.5. Also, the constituents are regrouped as $\alpha = m_s\beta^*$ in presenting the results in Section 3, so that the velocity factor v is eliminated. In order to account for the effect of mesh discretization, the near-tip mesh was successively refined until the temperature difference between two meshes at a certain point close to the tip was less than 5 percent. Also, in order to avoid unnecessary ambiguity due to mesh resolution, temperature results in Section 3 will be presented only at a small finite distance from the crack tip (and not at the crack tip itself).

3. Results and discussion

As mentioned above, for the purpose of discussing the results, a normalized viscosity parameter $\alpha = \beta^* m_s$ is employed. It is noted from (11) that α is independent of crack velocity and contains only the material parameters and the remote stress intensity factor K. As mentioned earlier in connection with β^*, smaller values of α correspond to greater amounts of rate sensitivity. Results are presented below for α values ranging from 2.5 to 20. This range of α values corresponds to K varying from 175 to $500\,\mathrm{MPa}\sqrt{m}$ for the material chosen in Section 2. These K values are typical for this material [32], over the range of crack speeds that is considered here.

The radial variation of the opening stress σ_{22}/σ_0 and plastic strain $\varepsilon^p_{22}/\varepsilon_0$ with respect to normalized distance ahead of the crack tip is shown in Figs. 1a–c and 2a–c, respectively.

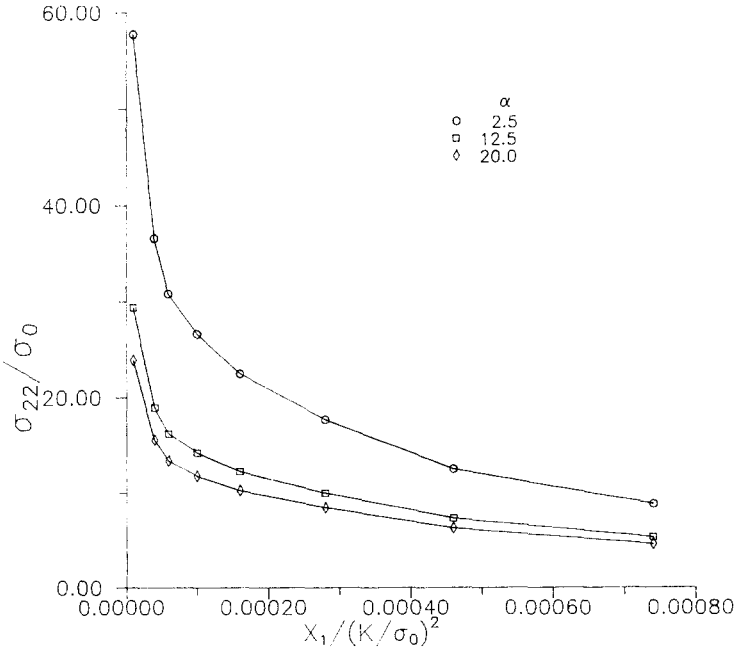

Fig. 1a. Stress variation ahead of the crack tip. $V/C_s = 0.1$.

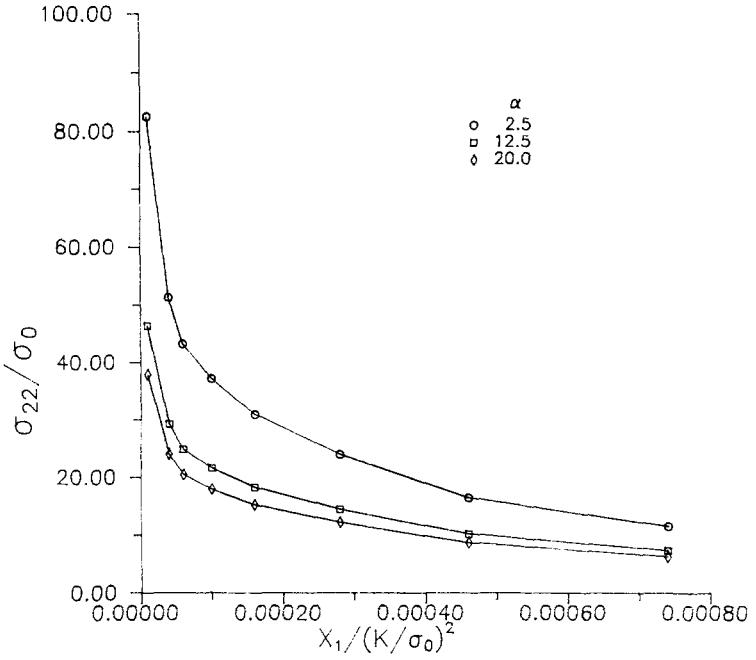

Fig. 1b. Stress variation ahead of the crack tip. $V/C_s = 0.3$.

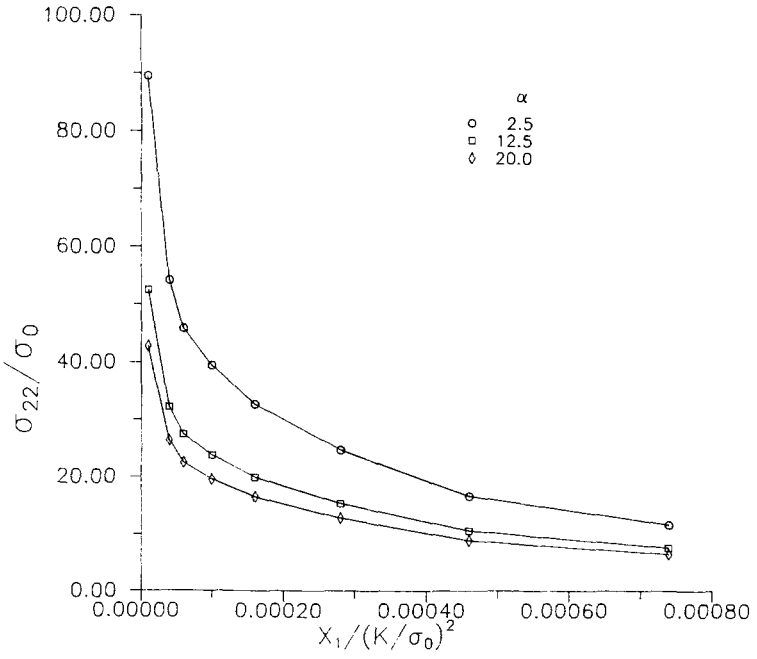

Fig. 1c. Stress variation ahead of the crack tip. $V/C_s = 0.5$.

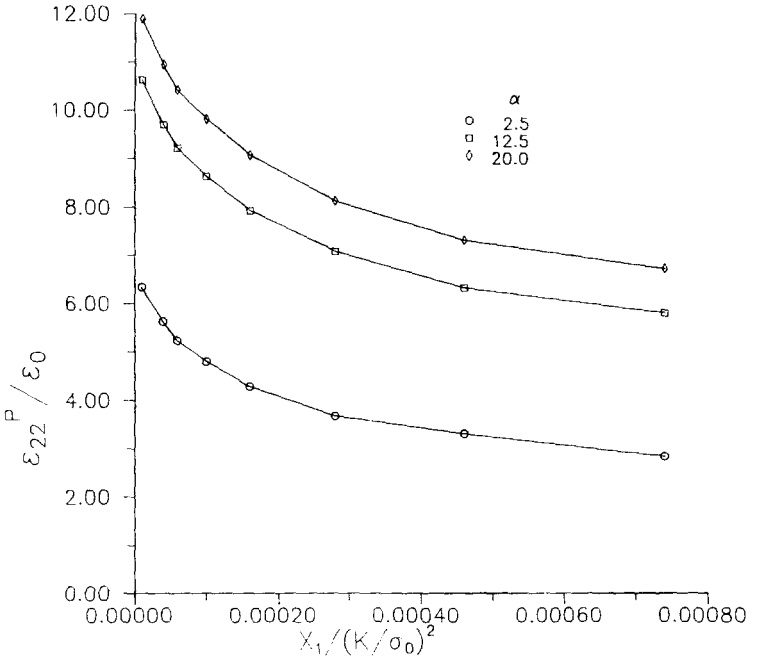

Fig. 2a. $\hat{\varepsilon}_{22}^{p}$ variation ahead of the crack tip. $V/C_s = 0.1$.

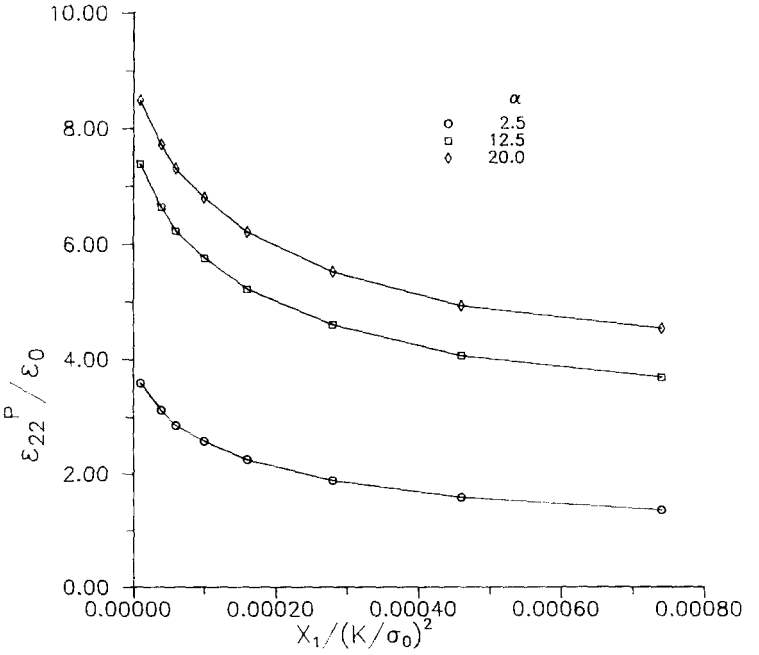

Fig. 2b. $\hat{\varepsilon}_{22}^{p}$ variation ahead of the crack tip. $V/C_s = 0.3$.

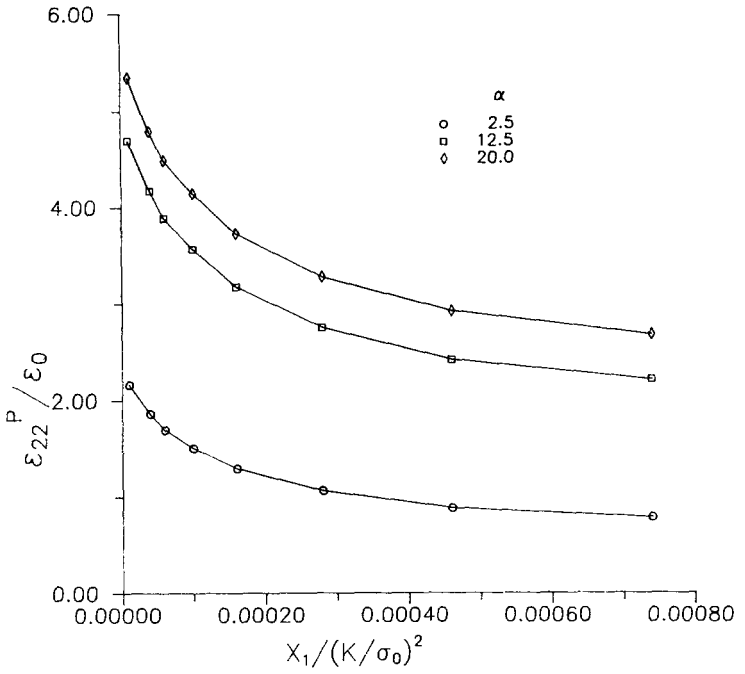

Fig. 2c. $\hat{\varepsilon}^p_{22}$ variation ahead of the crack tip. $V/C_s = 0.5$.

Results are displayed for different values of normalized viscosity parameter α and crack speeds m_s. It is seen from Fig. 1 that for $\alpha = 2.5$ the stress near the crack tip is higher and decreases with increasing α. In order to understand this result, it should be noted that materials with a high degree of rate sensitivity (low α values) can sustain larger stress levels in the vicinity of the crack tip, where strain rates are large. On the other hand, it may be observed from Fig. 2 that the plastic strain increases with α. As pointed out by Freund and Douglas [24], the lower plastic strains for materials with higher degrees of rate sensitivity may result in a dramatic increase in fracture toughness values, when crack propagation occurs by a ductile mechanism.

It can be noticed from Fig. 1 that σ_{22}/σ_0 corresponding to any fixed value of α increases strongly with crack speed for $m_s < 0.3$ (see Figs. 1a and 1b), and only marginally for $m_s > 0.3$ (see Figs. 1b and 1c). This is because at low crack speeds rate sensitivity plays an important role leading to an increase in stress with crack speed. However, for $m_s > 0.3$ material inertia becomes significant and opposes the influence of rate sensitivity in elevating the stress.

The effect of both rate sensitivity and material inertia is to decrease the plastic strains near the crack tip. The influence of the latter can be seen for high crack speeds (compare Figs. 2b and 2c). This has also been observed by Lam and Freund [15], Freund and Douglas [14] and Achenbach and Dunayevsky [17] for rate independent materials and Freund and Douglas [24] for rate dependent materials. It results in an increase in dynamic fracture toughness with crack speed for large crack speeds.

For low crack speeds ($m_s < 0.3$), it can be noticed from Figs. 2a and 2b that the plastic strain, ε^p_{22}, and its normalized gradient, $\partial\varepsilon^p_{22}/\partial\hat{x}_1$, display a sharper decrease with crack speed

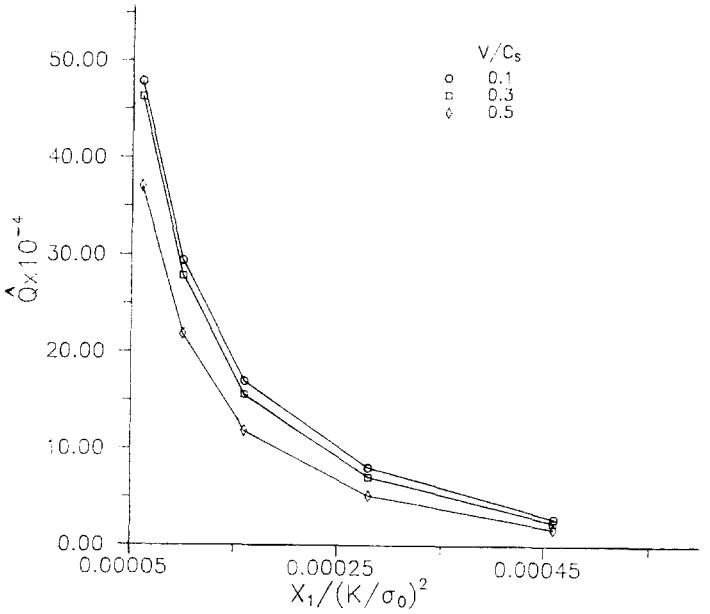

Fig. 3a. Variation of normalized work rate $\hat{Q}$ ahead of the crack tip. $\alpha = 2.5$.

when the α value is small. This sharp decrease in plastic strain for highly rate sensitive materials is expected to result in a rapid increase in fracture toughness with crack speed, when crack speeds are small and inertia effects are unimportant (see [24, 33]).

The radial variation of the normalized heat input, $\hat{Q} = -\hat{\sigma}_{ij}\hat{c}\hat{\varepsilon}^p_{ij}/\partial\hat{x}_1$, ahead of the crack tip corresponding to m_s values of 0.1, 0.3 and 0.5 is shown in Figs. 3a–c for three different α values. To facilitate easy interpretation, the temperature (rise) distribution ahead of the

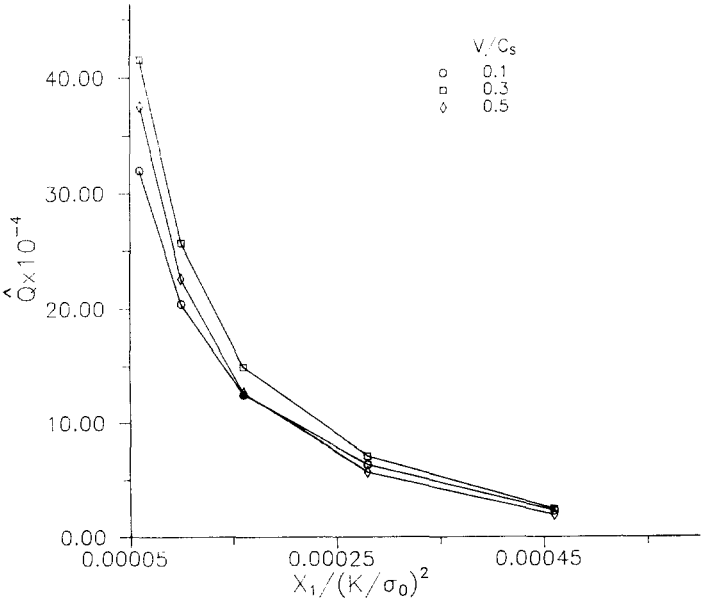

Fig. 3b. Variation of normalized work rate $\hat{Q}$ ahead of the crack tip. $\alpha = 12.5$.

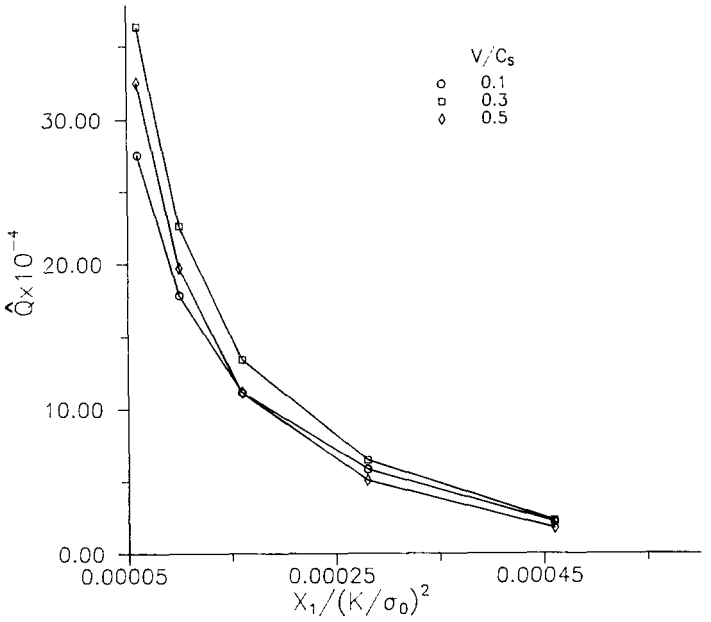

Fig. 3c. Variation of normalized work rate $\hat{Q}$ ahead of the crack tip. $\alpha = 20.0$.

crack tip is presented in a similar manner in Figs. 4a–c as a function of $\hat{x}_1$ for three different values of m_s and α. The corresponding temperature distribution directly *above* the crack tip with respect to $\hat{x}_2$ is displayed in Figs. 5a–c.

It is seen from Fig. 4 that the temperature rise is a strong function of the parameter α and the normalized crack speed m_s. From small α values, the temperature rise ahead of the crack tip is highest for low crack speeds (Fig. 4a). For example, corresponding to $\alpha = 2.5$, the temperature rise at $\hat{x}_1 = 5 \times 10^{-5}$ is 235°C, 200°C and 155°C for $m_s = 0.1$, 0.3 and 0.5 respectively. However, for large α values it is found from Fig. 4c that the temperature immediately in front of the crack tip initially increases with crack speed and then decreases. For example, corresponding to $\alpha = 20$, the temperature rise at $\hat{x}_1 = 5 \times 10^{-5}$ is 170°C, 190°C and 160°C for $m_s = 0.1$, 0.3 and 0.5 respectively.

In order to understand the above results, it is important to examine the magnitude of the three times involved in the governing heat conduction/convection equation (15). As mentioned earlier, the value of the Péclet number is large for the range of crack velocities considered here. Due to this, the convection term in (15) will dominate over the conduction term, provided that $\partial^2 T/\partial \hat{x}_1^2$ or $\partial^2 T/\partial \hat{x}_2^2$ is also not large. Hence, it follows from this equation that for points which are not at or very near the crack tip, the temperature may be well approximated by the following integral:

$$\Delta T(\hat{x}_1, \hat{x}_2) \approx \frac{\sigma_0^2}{E\rho c_p} \int_{\hat{x}_1}^{R_p(\hat{x}_2)} \hat{Q}(\xi, \hat{x}_2)\, \mathrm{d}\xi. \tag{18}$$

Here $R_p(\hat{x}_2)$ represents the distance to the elastic-plastic boundary from the crack tip in the positive $\hat{x}_1$ direction corresponding to a certain value of $\hat{x}_2$. The above approximate result may also be obtained by performing an asymptotic expansion of the integral representation given by Rice and Levy [3] which is based on the superposition of distributed sources.

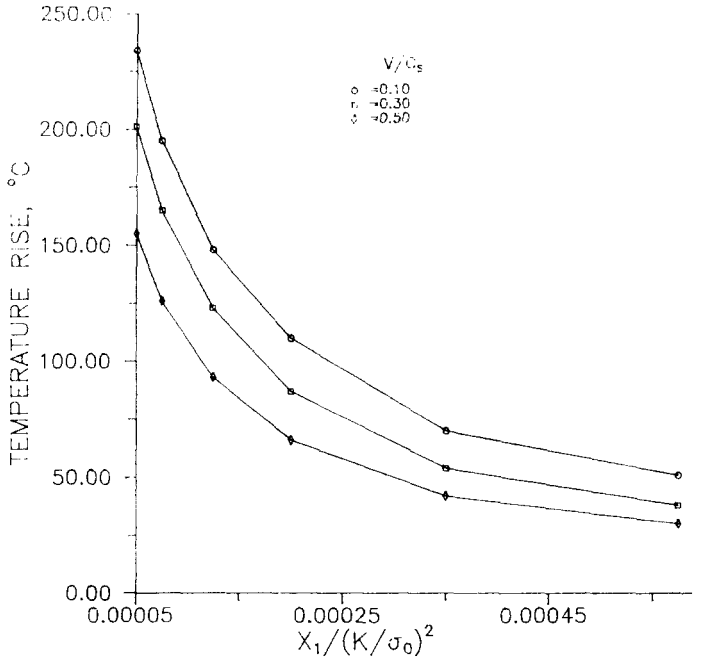

Fig. 4a. Temperature rise ahead of the crack tip. $\alpha = 2.5$.

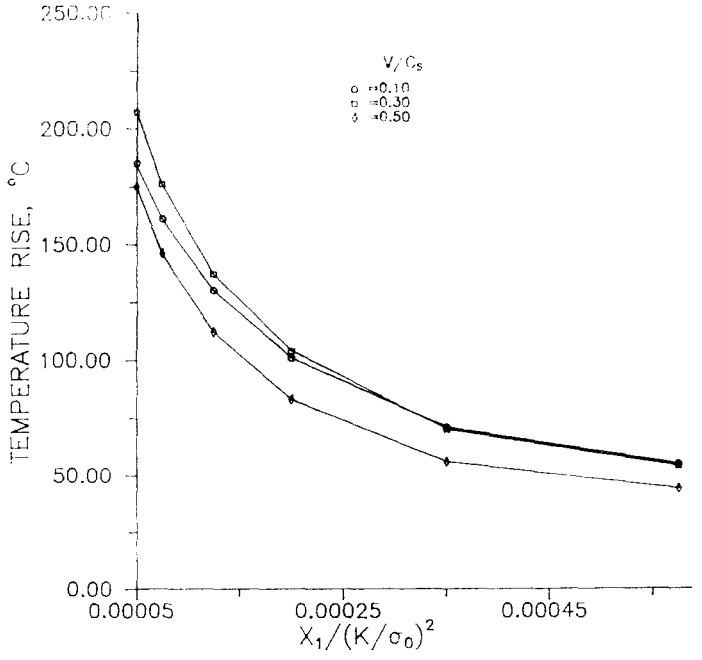

Fig. 4b. Temperature rise ahead of the crack tip. $\alpha = 12.5$.

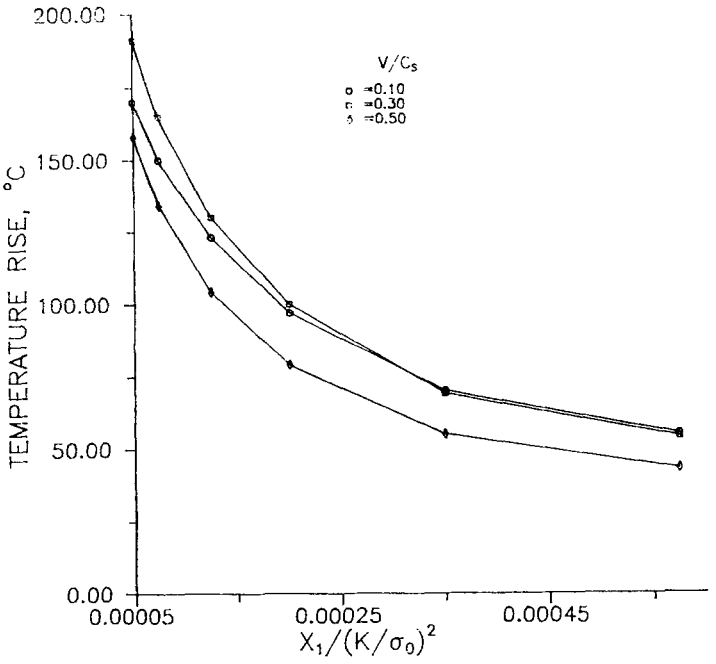

Fig. 4c. Temperature rise ahead of the crack tip. $\alpha = 20.0$.

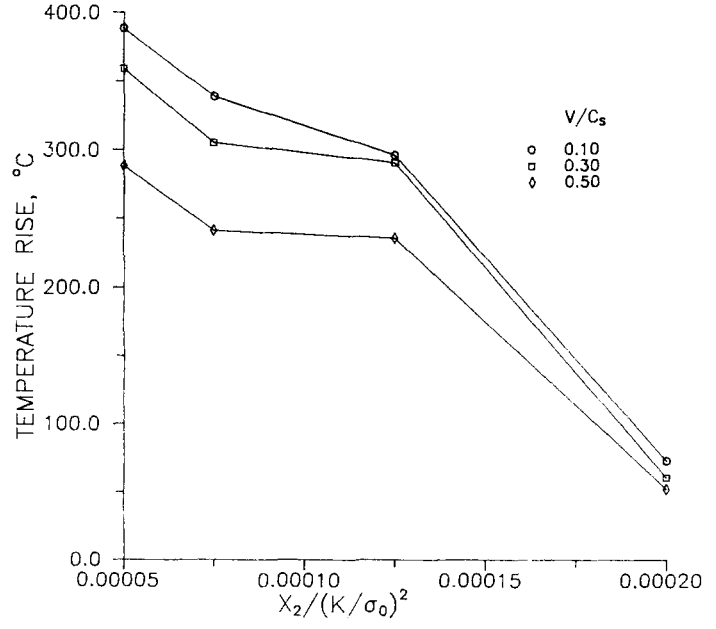

Fig. 5a. Temperature rise above the crack tip. $\alpha = 2.5$.

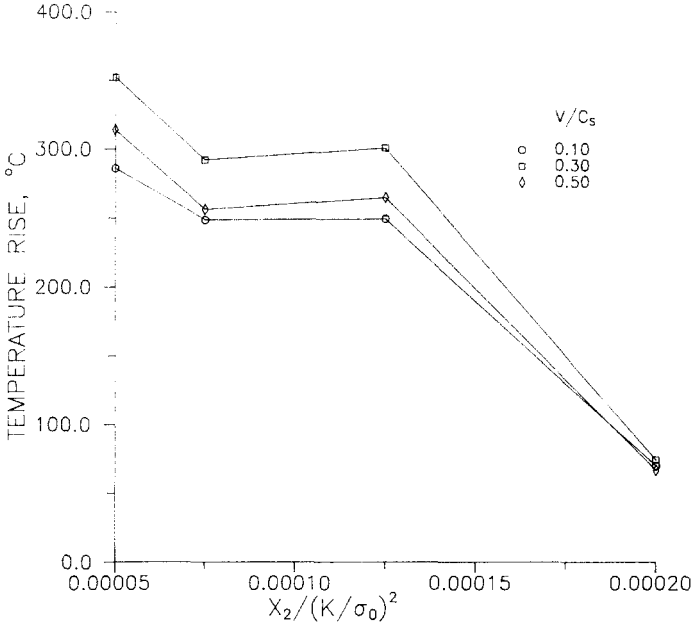

Fig. 5b. Temperature rise above the crack tip. $\alpha = 12.5$.

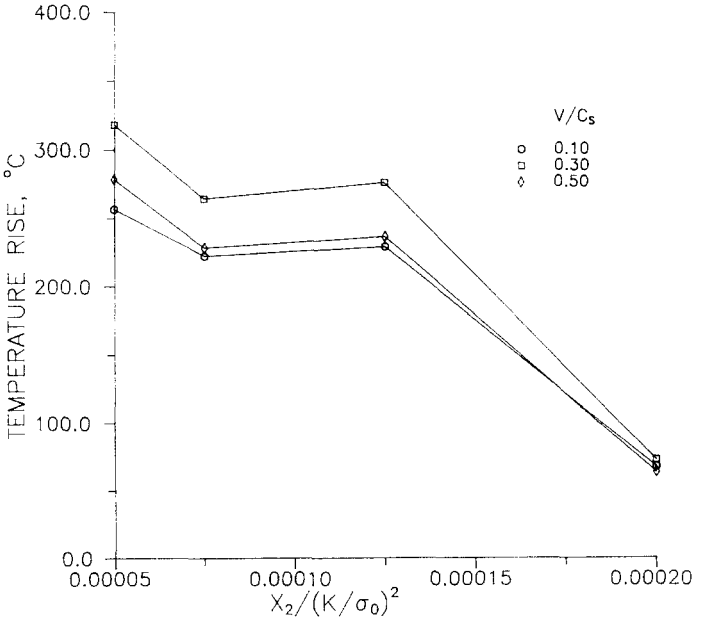

Fig. 5c. Temperature rise above the crack tip. $\alpha = 20.0$.

The variation of the normalized heat input $\hat{Q}$ ahead of the crack tip for a small α value ($\alpha = 2.5$) is shown in Fig. 3a, corresponding to different crack speeds. This figure shows that $\hat{Q}$ is highest for an m_s value of 0.1, which is followed by that for 0.3 and 0.5. The decrease in $\hat{Q}$ as m_s varies from 0.3 to 0.5 is attributed to inertial effects. On the other hand, $\hat{Q}$ decreases as m_s increases from 0.1 to 0.3 because rate effects are strong in this case and cause a sharp drop in the plastic strain gradient (see remarks made earlier in connection with Figs. 2a and 2b). This offsets the elevation in stress with crack speed.

As noted in the foregoing discussion, the effect of this variation in $\hat{Q}$ is reflected on the temperature distribution ahead of the tip shown in Fig. 4a. The temperature is found to be highest for $m_s = 0.1$, followed by that for $m_s = 0.3$ and 0.5. Also, the difference in temperature values between $m_s = 0.1$ and 0.3, as well as that between 0.3 and 0.5 increases as the crack tip is approached. These features in the temperature distribution are thus a consequence of (18).

For large values of α, it may be observed from Fig. 3c that $\hat{Q}$ *near* the crack tip is highest for $m_s = 0.3$. This is followed by the curves corresponding to $m_s = 0.5$ and 0.1. The increase in $\hat{Q}$ as m_s varies from 0.1 to 0.3 occurs because rate effects are mild in this case, and the decrease in plastic strain gradient is not sufficient to offset the elevation in stress with crack speed. At points *away* from the crack tip, $\hat{Q}$ is about the same for $m_s = 0.3$ and 0.1. This, however, is higher when compared with the curve for $m_s = 0.5$. These variations in $\hat{Q}$ influence the temperature distribution ahead of the crack tip in accordance with (18), as explained below.

It may be seen from Fig. 4c (for $\alpha = 20$) that the temperature corresponding to $m_s = 0.3$ and 0.1 is about the same and higher than that for 0.5 at points *away* from the crack tip. As the crack tip is approached, the difference in temperature between $m_s = 0.3$ and 0.1 increases, while that between $m_s = 0.1$ and 0.5 decreases.

On comparing Figs. 5a–c with Figs. 4a–c, it can be noticed that the temperature is higher as the crack tip is approached from above (i.e., along the $\hat{x}_2$ axis). Figure 5a shows that for a small α value, the temperature directly above the crack tip decreases as the crack speed increases. For example, corresponding to $\alpha = 2.5$, the temperature rise at $\hat{x}_2 = 5 \times 10^{-5}$ is 385°C, 360°C and 290°C for $m_s = 0.1$, 0.3 and 0.5 respectively. On the other hand, Fig. 5c illustrates that for a large α value, the temperature corresponding to an intermediate crack speed ($m_s = 0.3$) is higher than that for the extreme values of $m_s = 0.1$ and 0.5. Thus, corresponding to $\alpha = 20$, the temperature rise above the crack tip at $\hat{x}_2 = 5 \times 10^{-5}$ is 255°C, 320°C and 275°C for $m_s = 0.1$, 0.3 and 0.5 respectively.

The above study clearly indicates the importance of the parameter α and the (normalized) crack velocity m_s in determining the temperature distribution in a given viscoplastic material during dynamic crack growth.

Acknowledgement

The authors wish to acknowledge the computational facilities provided by the Department of Science and Technology (Government of India) under Project No. III. 4 (38)/85-ET. The second author would also like to thank the Aeronautical Research and Development Board (Government of India) for financial support through Project No. Aero/RD-134/100/10/88-89/519.

References

1. J.M. Krafft and G.R. Irwin, in *Symposium on Fracture Toughness Testing*, ASTM STP 381 (1965) 114–129.
2. J. Eftis and J.M. Krafft, *Journal of Basic Engineering* 87 (1965) 257–263.
3. J.R. Rice and N. Levy, in *The Physics of Strength and Plasticity*, M.I.T. Press, Cambridge (1969) 277–298.
4. R. Weichert and K. Schonert, *Journal of Mechanics and Physics of Solids* 22 (1974) 127–133.
5. R. Weichert and K. Schonert, *Journal of Mechanics and Physics of Solids* 26 (1978) 151–161.
6. Z.B. Kuang and S.N. Atluri, *Journal of Applied Mechanics* 52 (1985) 274–280.
7. A.S. Douglas and H.U. Mair, *Scripta Metallurgica* 21 (1987) 479–484.
8. P.N. Malali, Thermal Fields Generated by Dynamic Mode III Fracture in Ductile Materials, M.S. thesis, The Johns Hopkins University, Baltimore (1988).
9. H.S. Carslaw and J.C. Jaeger, *Conduction of Heat in Solids*, Oxford University Press, Oxford (1959).
10. K.N.G. Fuller, P.G. Fox and J.E. Field, *Proceedings of the Royal Society (London)* A341 (1975) 537–557.
11. A.T. Zehnder and A.J. Rosakis, On the Temperature Distribution at the Vicinity of Dynamically Propagating Cracks in 4340 Steel, GALCIT Report SM 89-2, California Institute of Technology, Pasadena (1989).
12. P.J. Loos and F.R. Brotzen, *Scripta Metallurgica* 17 (1983) 389–392.
13. P.J. Loos and F.R. Brotzen, *Metallurgical Transactions A* 14A (1983) 1409–1419.
14. L.B. Freund and A.S. Douglas, *Journal of Mechanics and Physics of Solids* 30 (1982) 59–74.
15. P.S. Lam and L.B. Freund, *Journal of Mechanics and Physics of Solids* 33 (1985) 153–174.
16. L.I. Slepyan, *Izvestiya Akademii Nauk SSSR, Mekhanika Tverdogo Tela* 11 (1976) 126–134 (English Translation).
17. J.D. Achenbach and V. Dunayevsky, *Journal of Mechanics and Physics of Solids* 29 (1981) 283–303.
18. Y.C. Gao and S. Nemat-Nasser, *Mechanics of Materials* 2 (1983) 47–60.
19. Q. Guo, Z. Li and K. Li, *International Journal of Fracture* 36 (1988) 71–82.
20. K.K. Lo, *Journal of Mechanics and Physics of Solids* 31 (1983) 287–305.
21. L.B. Freund and J.W. Hutchinson, *Journal of Mechanics and Physics of Solids* 33 (1985) 169–191.
22. L.B. Freund, J.W. Hutchinson and P.S. Lam, *Engineering Fracture Mechanics* 23 (1986) 119–130.
23. B. Brickstad, *Journal of Mechanics and Physics of Solids* 31 (1983) 307–327.
24. L.B. Freund and A.S. Douglas, in *Elastic-Plastic Fracture: Second Symposium Vol. I-Inelastic Crack Analysis*, ASTM STP 803 (1983) 5–20.
25. P. Perzyna, in *Advances in Applied Mechanics*, Academic Press, New York 9 (1966) 243–377.
26. J.C. Sung and J.D. Achenbach, *Journal of Thermal Stresses* 10 (1987) 243.
27. L.B. Freund, in *Mechanics Today*, Pergamon Press, New York (1976) 55–91.
28. D. Pierce, C.F. Shih and A. Needleman, *Computers and Structures* 18 (1984) 875–887.
29. B. Moran, *Computers and Structures* 27 (1987) 237–240.
30. O.C. Zienkiewicz, *The Finite Element Method* (3rd ed.), McGraw Hill, U.K. (1977).
31. A.N. Brooks and T.J.R. Hughes, *Computer Methods in Applied Mechanics and Engineering* 32 (1982) 199–259.
32. L. Dahlberg, F. Nilsson and B. Brickstad, in *Crack Arrest Methodology and Applications*, ASTM STP 711 (1980) 89–108.
33. P.A. Mataga, L.B. Freund and J.W. Hutchinson, *Journal of Physics and Chemistry of Solids* 48 (1987) 985–1005.